

# A numerical model for the Serpens radio jet

A.C. Raga<sup>1</sup>, S. Curiel<sup>1</sup>, L.F. Rodríguez<sup>2</sup>, and J. Cantó<sup>1</sup>

<sup>1</sup> Instituto de Astronomía, UNAM, Apartado Postal 70-264, 04510 D.F., México (raga@astroscu.unam.mx)

<sup>2</sup> Instituto de Astronomía, UNAM, Campus Morelia, Apdo. Postal 3-72 (Xangari), Morelia, Michoacán 58089, México

Received 13 June 2000 / Accepted 31 August 2000

**Abstract.** The Serpens (“triple source”) radio continuum jet shows a series of aligned knots with  $\approx 1\text{--}2''$  angular separations, forming a curved structure circumscribed within a cone of  $\sim 10^\circ$  full opening angle. We present a high resolution, 3D numerical simulation of a jet with variable ejection direction and velocity with parameters appropriate for the Serpens jet, from which we obtain predictions of 3.6 cm radio continuum maps. We find that the general morphology of the radio emission, and the time evolution of the successive knots, qualitatively agree with 3.6 cm VLA observations of the Serpens radio jet.

**Key words:** hydrodynamics – molecular processes – radiative transfer – ISM: clouds – ISM: Herbig-Haro objects – ISM: jets and outflows

## 1. Introduction

The Serpens triple radio source (Rodríguez et al. 1980; Snell & Bally 1986) coincides with the FIRS 1 (IRAS 18273+0113) far infrared source (Harvey et al. 1984), but has not been detected at near infrared nor optical wavelengths (Zeiner & Eisloffel 1999). The region around this source has been mapped in lines of the  $\text{NH}_3$  molecule, and has peculiar kinematics which are probably a result of the interaction of the triple source with the surrounding environment (Torrelles et al. 1992; Curiel et al. 1996). Single-dish and interferometric line observations of other molecules have also shown a dense molecular core around this radio continuum source, as well as widespread outflow activity (e.g., McMullin et al. 1994; White et al. 1995).

The triple radio continuum source itself has most interesting properties. One of the notable features is that some regions of this object appear to show a partial contribution from a non-thermal component (as evidenced by a negative spectral index, Rodríguez et al. 1989). This result has prompted theoretical studies of the acceleration of relativistic electrons in shocks related to outflows from young stars (Crusius-Wätzel 1990; Henriksen et al. 1991). In more recent observational work, Curiel et al. (1993) concluded that even though there appears to be an extended non-thermal component, most of the emission that

one observes from the knots in the triple radio source appears to correspond to a thermal, free-free radio continuum.

The most remarkable property of the triple source are the large proper motions of its outer components. While the central component does not show a detectable proper motion, the main two outer components move away from the central source with velocities of  $\sim 200 \text{ km s}^{-1}$  (Rodríguez et al. 1989; Curiel et al. 1993, 1996). This result leads to a possible interpretation of this object as a young star (coinciding with the position of the central component) ejecting a bipolar jet system. Far infrared, sub-millimeter and millimeter observations have revealed that this object is very young, having characteristics of a class 0 protostar (e.g., Casali et al. 1993; Hurt & Barsony 1996). More recent radio continuum observations (Curiel et al. 1993) show that the NW lobe of the Serpens jet actually has a chain of four or five aligned knots, resulting in a morphology that closely resembles optically detected Herbig-Haro (HH) jets (such as HH 34 or HH 111, see, e. g., Reipurth et al. 1997), though having a spatial extent which is smaller by about an order of magnitude.

Curiel et al. (1993) interpreted the structure of the Serpens triple radio continuum source as a bipolar jet from a precessing source. In the present paper, we explore this possibility by first computing the parameters necessary for explaining the observed structure with a model of a precessing, variable ejection velocity jet (Sect. 2). We then compute a 3D numerical simulation with these parameters, from which we obtain predicted radio continuum maps that can be directly compared with the observations (Sect. 3). Finally, we discuss the relative success of this model at reproducing the radio continuum observations of the Serpens triple radio source (Sect. 4).

We should note that both analytic (Raga et al. 1993) and numerical models (Cox et al. 1991; de Gouveia dal Pino & Benz 1993; Biro et al. 1995; Cliffe et al. 1996) of HH jets from precessing sources have been studied in the past. Also, the problem of a jet with a general velocity+direction ejection variability has been studied (analytic considerations and 2D numerical models are presented by Raga & Biro 1993). Finally, a number of 3D numerical simulations of HH jets from variable sources have been carried out (e.g., Stone & Norman 1994; Suttner et al. 1997), and some of them include a small precession of the outflow in

order to break the axisymmetry of the jet (de Gouveia dal Pino et al. 1996; Völker et al. 1999).

## 2. The parameters for the Serpens jet

Very Large Array (VLA) 3.6 cm radio continuum maps of the NW lobe of the Serpens “triple source” jet obtained at three different epochs are shown in Fig. 1. These radio continuum observations were carried out with the 27 antennae of the Very Large Array (VLA) of the National Radio Astronomy Observatory (NRAO)<sup>1</sup> in its A-configuration at 3.6 cm in 1990 (June 1), 1995 (July 13), and 1998 (May 9). These data are part of a long term monitoring program in progress of this remarkable radio continuum jet, and the technical details of the observations will be given in Curiel et al. (2000). The data were edited and calibrated following standard VLA procedures with AIPS. The maps of the three different epochs were made by weighting the  $(u, v)$  data with the Briggs (1995) “robustness” parameter set to 4 to enhance weak knots and faint extended emission along the radio jet, which yielded a synthesized beam of about  $0.''42 \times 0.''38$  and an rms noise of about  $17 \mu\text{Jy}$ , with small variations at each epoch. The maps were rotated 48.55 degrees counterclockwise in order to align the NW radio lobe with the vertical axis.

This system actually has two lobes (the southern lobe not being shown in Fig. 1), both having proper motion velocities of  $\approx 200 \text{ km s}^{-1}$  away from the central source (Curiel et al. 1993). As there are no radial velocity measurements for this purely continuum jet, we are forced to assume that the outflow axis lies on the plane of the sky, and that the measured proper motions therefore indicate that the jet has a velocity of  $\approx 200 \text{ km s}^{-1}$ .

The NW lobe shows 5 well defined knots (see Fig. 1), with separations of  $\approx 1.5''$ , corresponding to a projected distance of  $\approx 7 \times 10^{15} \text{ cm}$  (at a distance of 300 pc for the Serpens star formation region). If we want to model these knots as the result of an ejection velocity time-variability, the period of this variability has to have a value of  $\tau_v \approx 7 \times 10^{15} \text{ cm} / 200 \text{ km s}^{-1} \approx 10 \text{ yr}$ . Similar periods have been determined for the moving knots in HH 80-81 (Martí et al. 1995) and HH 1-2 (Reipurth et al. 2000).

The amplitude of the time-variability can be constrained as follows. From the analytic theory for the formation of working surfaces, one obtains that for an ejection velocity variability of the form:

$$u_0(t) = v_0 + \Delta v \sin\left(\frac{2\pi t}{\tau_v}\right), \quad (1)$$

the working surfaces first appear at a distance

$$x_c \approx \frac{v_0^2 \tau_v}{2\pi \Delta v} \quad (2)$$

from the source. This simple expression is strictly valid for  $\Delta v \ll v_0$ , with the exact value for  $x_c$  being given by Raga & Noriega-Crespo (1998).

<sup>1</sup> NRAO is a facility of the National Science Foundation operated under cooperative agreement by Associated Universities, Inc.

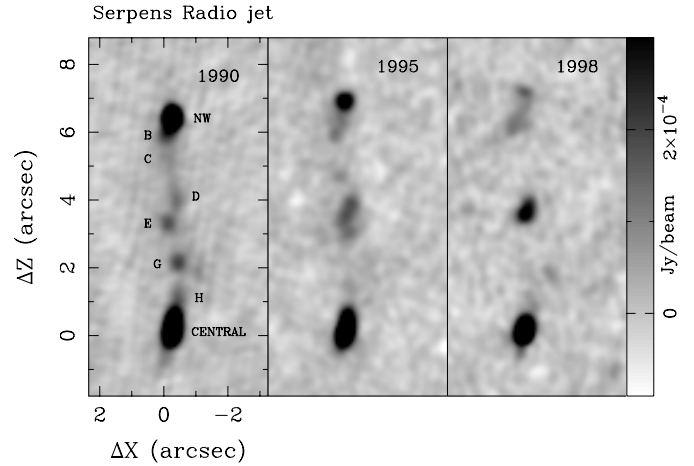


**Fig. 1.** 3.6 cm VLA radio continuum maps of the NW lobe of the Serpens radio jet obtained at three different epochs. The ordinate is aligned with a NW direction (PA=  $48^\circ.55$ ). The proper motions and intensity variations of the knots along the jet can be clearly seen. The axes are labeled in arcseconds, with the zero point corresponding to the position of the outflow source. The identification of the radio knots was taken from Curiel et al. (1993).

Now, the first well defined knot in the NW lobe of the Serpens jet (see Fig. 1) is at a distance of  $\approx 1''$  from the source. However, there is an extension of the source emission of  $\approx 0.5''$  to the NW, which appears to represent the next knot forming along this outflow. This implies that the knots are formed at a distance of  $\sim 2.5 \times 10^{15} \text{ cm}$  from the source. If we take this value as an estimate for  $x_c$ , we can use our estimates of  $v_0 \approx 200 \text{ km s}^{-1}$  and  $\tau_v \approx 10 \text{ yr}$  to derive an amplitude of  $\Delta v \approx 80 \text{ km s}^{-1}$ .

In this way, we have selected parameters for a sinusoidal ejection velocity variability (Eq. 1), which are consistent with the knot spacings and proper motions observed for the NW lobe of the Serpens jet. The most uncertain parameter is the amplitude  $\Delta v$  of the variability, as this amplitude depends on the distance  $x_c$  from the source at which the knots first appear, which cannot be reliably determined from the observations.

In the 3.6 cm maps (Fig. 1) it is clearly seen that the knots in the NW lobe appear to trace a precession cone. The full opening angle of this cone has a value of  $\alpha \approx 10^\circ$  (Curiel et al. 1993, 1996). From the morphology of the jet, one sees that the precession period has to be similar to the dynamical timescale of the leading condensation (see Fig. 1). Therefore, the precession period has a value  $\tau_p \approx 6''.5 / 200 \text{ km s}^{-1} \approx 50 \text{ yr}$ .

It is difficult to estimate the density of the jet and the environment directly downstream of the leading condensations of the two lobes of the Serpens outflow. Given the fact that these condensations have high proper motions, similar to those of the inner condensations (see Curiel et al. 1993), one would conclude that either the environment has a rather low density compared to the jet (for example, the jet could be moving into a cavity which was partially evacuated by previous outflow episodes), or that the jet is moving into (undetected) moving material which was previously ejected from the source. Molecular observations of

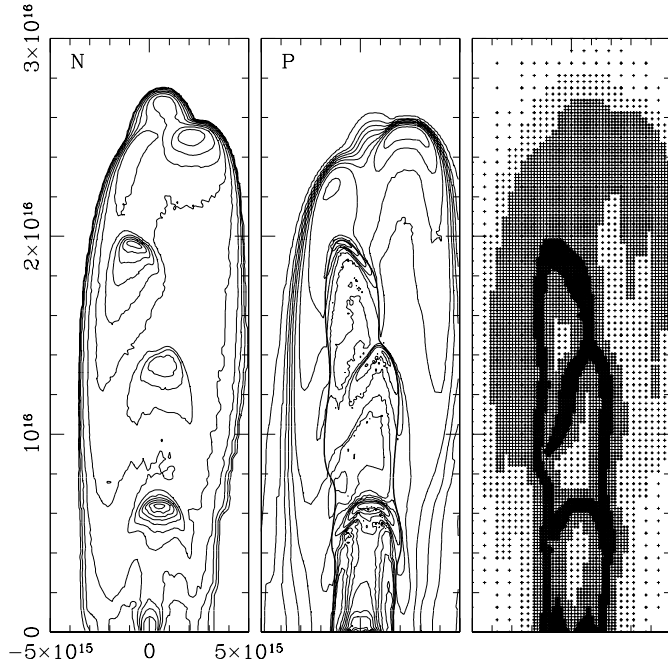


**Fig. 2.** Column density (left, factor of  $\sqrt{2}$  contours), pressure stratification on the central,  $y = 0$  plane of the outflow (centre, factor of 2 contours) and the points on this plane chosen by the adaptive grid algorithm (right), for the flow obtained after a 60 yr time-integration. The thick contour in the pressure plot (centre) delineates the contact discontinuity separating the jet from the environmental material. The axes are labeled in cm.

the dense core indicate that the ambient gas density is probably several times  $10^4 \text{ cm}^{-3}$ , or even higher than  $10^5 \text{ cm}^{-3}$  (e.g., Curiel et al. 1996; McMullin et al. 1994). Assuming that the radio emission comes from  $\sim 200 \text{ km s}^{-1}$  shocks inside the jet beam, Curiel et al. (1993) estimate a jet density  $n_j \sim 10^4\text{--}10^5 \text{ cm}^{-3}$ . To summarize, it appears that the radio continuum jet is moving into a low density cavity, or into previously ejected material, and that the jet density is in the  $n_j \sim 10^4\text{--}10^5 \text{ cm}^{-3}$  range.

Finally, the knots along the NW lobe of the Serpens outflow are at most marginally resolved across the outflow axis. This leads to an estimate of  $\sim 5 \times 10^{14} \text{ cm}$  for the jet radius.

### 3. The model

We compute a numerical model of a jet with a sinusoidal variable ejection velocity of period  $\tau_v = 10 \text{ yr}$ , half-amplitude  $\Delta v = 80 \text{ km s}^{-1}$  and mean velocity  $v_0 = 200 \text{ km s}^{-1}$  (see Eq. 1). The injection velocity has a direction at an angle of  $5^\circ$  from the  $z$ -axis, initially lying on the  $xz$ -plane, and then precessing around the  $z$ -axis with a precession period  $\tau_p = 50 \text{ yr}$ . We also impose an initial jet radius  $r_j = 5 \times 10^{14} \text{ cm}$ . These parameters are consistent with the VLA observations of the Serpens triple radio source (see Sect. 2).

We choose an initial jet density of  $n_j = 10^4 \text{ cm}^{-3}$  and a  $n_{env} = 10^3 \text{ cm}^{-3}$ , uniform density for the surrounding environment (this low environmental density being chosen so that

the leading working surface of the jet can propagate at a high velocity through the computational grid). We have chosen a jet density consistent with the lower boundary of the density range estimated by Curiel et al. (1993, also see Sect. 2) in order to have as good a resolution of the post-shock cooling regions as possible.

We assume that both the jet and the environment are initially neutral, and that both have an initial temperature of  $10^3 \text{ K}$  (the precise value for this temperature not being important, since the Mach number of the flow is very high and all of the shocks are strong).

The numerical simulation is carried out with the 3D adaptive grid code “yguazú-a”, which is described in detail by Raga et al. (2000). In the configuration which has been used for the calculation, the code integrates the 3D gasdynamic equations, an advection equation for a passive scalar (with which different regions of the flow can be labeled), and a rate equation for the ionization of hydrogen. The simple cooling function discussed by Raga et al. (1999) has been included in the energy equation.

The calculation is done on a hierarchical, binary adaptive grid with a maximum resolution of  $7.81 \times 10^{13} \text{ cm}$  (along the three axes). The maximum resolution is only allowed in the region of space occupied by the material originally coming from the jet, and the region filled by environmental material is resolved at most with a grid of  $1.56 \times 10^{14} \text{ cm}$  spacing. The resulting grid structure is illustrated in Fig. 2.

The flow stratification obtained after a  $t = 60 \text{ yr}$  time-integration is shown in Fig. 2, where we display the column density (integrated along the  $y$ -axis), and the pressure stratification on the  $xz$ -plane. The grid points on this plane (chosen by the adaptive grid algorithm) are also shown. In this figure, one can clearly see four separate working surfaces. The leading working surface has a complex structure which results from the merger of a number of knots that catch up with the leading bow shock of the jet.

Figs. 3 and 4 show the 3.6 cm, free-free continuum maps predicted from the numerical jet model for different integration times. The maps have been computed assuming that the  $xz$ -plane coincides with the plane of the sky. In Fig. 3, we see the knots which are produced by the ejection velocity variability travelling down the jet flow, and eventually catching up with the leading bow shock. The successive knots travel in different directions, as a result of the precession.

It is clear that the knots show a complex time-evolution. In Fig. 4, we see that over a period of 10 years knot F becomes fainter (for  $t > 60 \text{ yr}$ ). Knot D also fades away, but knot E becomes brighter with increasing time. Knot D, however, had shown a dramatic intensity increase for  $t = 40 \rightarrow 60 \text{ yr}$  (see Fig. 3).

These complex changes in radio continuum intensity are illustrated in Fig. 5, where we show the 3.6 cm emission integrated along the  $x$ -axis. The resulting intensity vs. position curves show that while at some times the emission of the whole outflow lobe is dominated by a single knot (e.g., at  $t = 60 \text{ yr}$ , see Fig. 5), at other times several knots of comparable intensities are observed (e.g., at  $t = 40$  and  $70 \text{ yr}$ ).

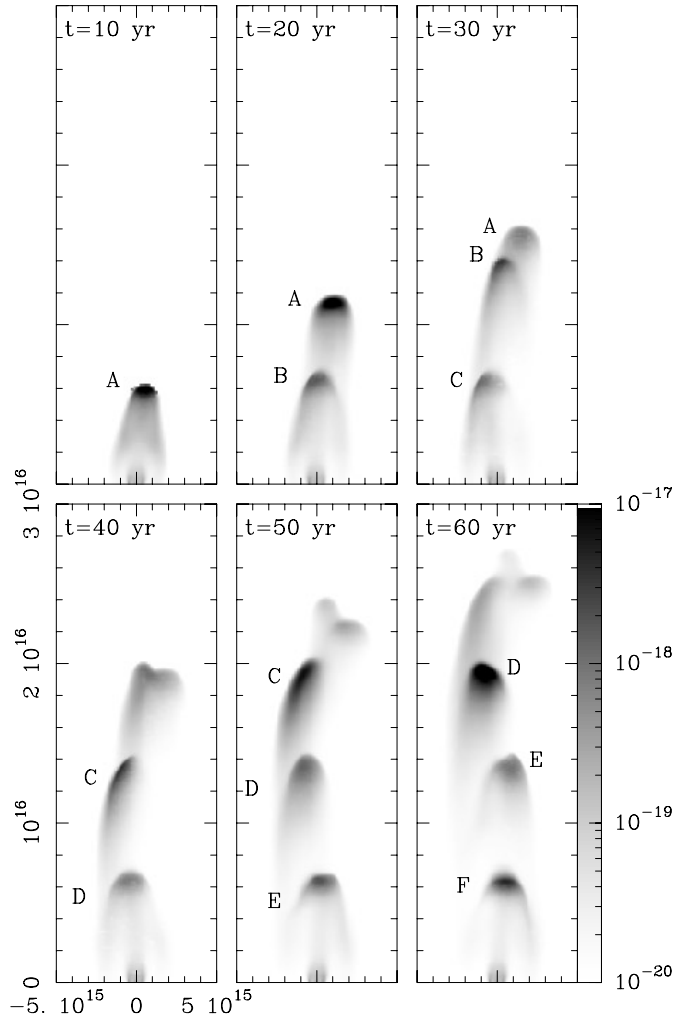


**Fig. 3.** 3.6 cm radio continuum maps predicted from the numerical jet model for integration times from 10 to 60 years. The greyscales are logarithmic, with the range shown by the wedge (in  $\text{erg s}^{-1} \text{cm}^{-2} \text{Hz}^{-1} \text{sterad}^{-1}$ ). The axes are labeled in cm. The successive working surfaces formed along the jet flow are labeled A through F, in order to identify the individual knots as they travel down the jet flow.

Given the extreme complexity of the flow, it is hard to understand in detail the light curves obtained for the successive knots. As pointed out by Raga & Noriega-Crespo (1998), the knots produced by a time-dependent ejection velocity have an intensity that first increases, and then decreases as the knots travel away from the source.

In the present simulation, this effect is combined with the precession, which becomes more important at larger distances from the source (Raga et al. 1993). As the knots diverge from each other at larger distances from the source (Raga & Biro 1993), the trailing knots eventually cross the bow shock wings of previously ejected knots. These interactions lead to brightenings of the knots.

A more dramatic effect is seen when the trajectory of one of the knots intersects the leading bow shock of the outflow. This

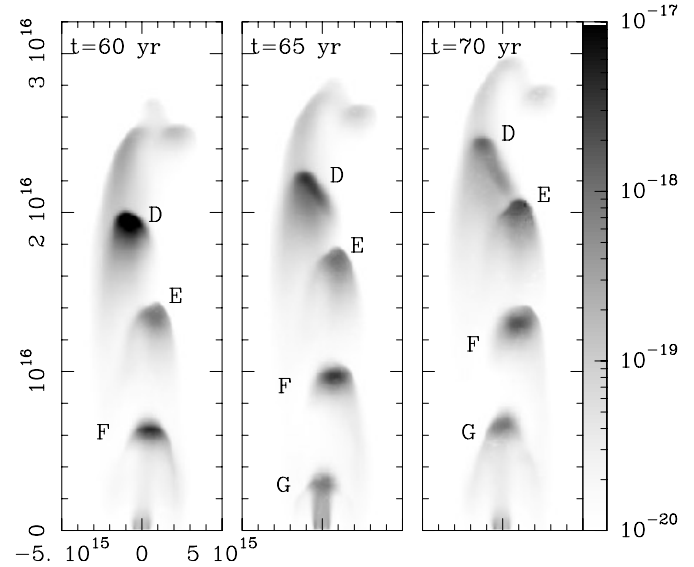


**Fig. 4.** 3.6 cm radio continuum maps predicted from the numerical jet model for integration times from 60 to 75 years (also see Fig. 3). The greyscales are logarithmic, with the range shown by the wedge (in  $\text{erg s}^{-1} \text{cm}^{-2} \text{Hz}^{-1} \text{sterad}^{-1}$ ). The axes are labeled in cm.

is seen for knot C in the  $t = 50$  yr map, and for knot D in the  $t = 60$  yr map (see Fig. 3).

A qualitative comparison of these results with the 3.6 cm VLA maps of the Serpens jet is presented in the following section.

#### 4. Discussion

From the 3.6 cm continuum VLA maps of the Serpens triple source, we have derived the parameters for an ejection velocity variability and a precession of the outflow axis that would be necessary for explaining the observed proper motions, knot spacings, and curved structure of the NW lobe of this object. With these parameters, we then compute a numerical simulation of a jet, from which we obtain predicted 3.6 cm free-free continuum maps which can be directly compared with the VLA observations.

The predicted maps show a morphology of emitting knots aligned along a curved trajectory, which agrees qualitatively well with the observations of the Serpens jet. This is not surprising, as the ejection velocity variability and the precession of the model jet were specifically chosen so as to obtain as good an agreement as possible.

However, we should point out that the 3.6 cm fluxes predicted from our model jet are considerably fainter than the ones observed for the Serpens jet. For example, the brighter knots in the model jet would have fluxes (at a distance of 300 pc) of  $\sim 0.01$  mJy/beam (if the knots are unresolved). This is approximately a factor of  $\sim 50$  lower than the fluxes of the brighter knots in the NW lobe of the Serpens jet (see Fig. 1).

This discrepancy between the model and the observations can be removed by increasing the jet density, and/or by increasing the mean velocity and amplitude of the time-dependent ejection

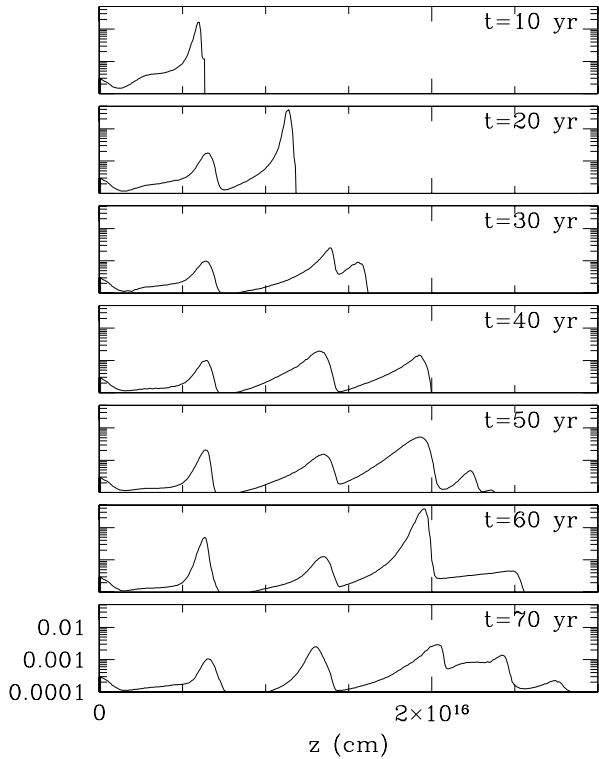


**Fig. 5.** 3.6 cm radio continuum emission integrated across the width of the outflow in the maps predicted from the numerical jet model (see Figs. 3 and 4) for integration times from 10 to 70 years. The emission is given in  $\text{erg s}^{-1} \text{cm}^{-1} \text{Hz}^{-1} \text{sterad}^{-1}$ .

tion velocity variability. For example, an increase of an order of magnitude in the jet density, and an amplitude for the ejection velocity variability about 50% larger than the one used in the numerical simulation, would bring the predicted fluxes up to the values observed in the Serpens jet. This results from the fact that the radio continuum scales approximately like the  $\text{H}\alpha$  intensity, which is approximately proportional to the preshock density times the shock velocity to the power 3.8 (see Raga & Kofman 1992). Such changes in the jet parameters would be reasonable, since for our numerical simulation we have chosen the lower boundary of the density range determined by Curiel et al. (1993), and for the velocity we have chosen the proper motions determined for the Serpens jet (the real velocities of course being higher as a result of projection effects).

Interestingly, the knots in the model jet show strong variabilities over periods of  $\sim 5$ -10 years (see Figs. 3–5). Due to the complex shock structures that result from the ejection variability, a given knot can have a series of brightening and fading away episodes over a time span of a few decades.

These complex time histories for the different knots result in qualitatively different morphologies for the jet. For example, at some times the jet has a bright, leading condensation, trailed by a chain of fainter knots closer to the source. Quite rapidly, this configuration can evolve into a structure in which one of the intermediate knots is completely dominant, or into a structure with several knots of comparable intensities (see Figs. 3–5).

The VLA maps of the Serpens triple source appear to show dramatic variabilities, which qualitatively resemble the ones of the model jet. For example, in 1990 the leading condensation of the NW lobe was much brighter than the rest of the knots, and by 1998 one of the intermediate knots had become dominant (see Fig. 1). The timescale of this variability is in good agreement with the model predictions.

This result is most interesting, because one of the important features of models of jets from variable sources is the resulting variability of the predicted jet structure. Even though detailed models for at least one HH jet have been computed (HH 34, Raga & Noriega-Crespo 1998), the comparison with the observations has not included an analysis of the observed time-evolution. Actually, very few observations of the time-variability of the optical emission of HH jets have been made, since the relevant timescales are of a few decades (Herbig 1969).

The situation is different for the very compact radio continuum jet in Serpens, for which the variability timescales are of only a few years. These timescales are similar to the ones found in some of the “microjets” from T Tauri stars (Burrows et al. 1996; Lavalley-Fouquet et al. 2000). The shorter timescales relevant for these objects do allow observational studies of the evolution of the intensities of the knots along the jets, and direct comparisons with predictions from time-dependent jet models. As far as we are aware, the work described above is the first effort at carrying out such comparisons between the predicted and observed time history of a jet from a young star.

*Acknowledgements.* We thank Sylvie Cabrit (the referee) for helpful comments about this paper. The work of AR and JC was supported by the CONACyT grants 32753-E and 27546-E. LFR acknowledges support from DGAPA (UNAM) and CONACyT (México).

## References

- Biro S., Raga A.C., Cantó J., 1995, MNRAS 275, 557
- Briggs D.S., 1995, Ph.D. Thesis, New Mexico Inst. Mining Tech.
- Burrows C.J., et al., 1996, ApJ 473, 437
- Casali M.M., Duncan W.D., 1993, 275, 195
- Cliffe J.A., Frank A., Jones T.W., 1996, MNRAS 282, 1114
- Cox C.L., Gull S.F., Scheuer P.A.G., 1991, MNRAS 252, 558
- Crusius-Wätzel A.R., 1990, ApJ 361, L49
- Curiel S., Rodríguez L.F., Gómez J.F., et al., 1996, ApJ 456, 677
- Curiel S., Rodríguez L.F., Cantó J., Moran J., 2000, in preparation
- Curiel S., Rodríguez L.F., Moran J.M., Cantó J., 1993, ApJ 415, 191
- de Gouveia dal Pino E.M., Benz W., 1993, ApJ 410, 686
- de Gouveia dal Pino E.M., Birkinshaw M., Benz W., 1996, ApJ 460, L111
- Harvey P.M., Wilking B.A., Joy M., 1984, ApJ 278, 156
- Henriksen R.N., Ptuskin V.S., Mirabel I.F., 1991, A&A 248, 221
- Herbig G.H., 1969, In: Detre L. (ed.) Non-Periodic Phenomena in Variable Stars. Reidel, p. 75
- Hurt R., Barsony M., 1996, ApJ 460, L45
- Lavalley-Fouquet C., Cabrit S., Dougados C., 2000, A&A 356, L41
- MartíJ., Rodríguez L.F., Reipurth B., 1995, ApJ 449, 184
- McMullin J.P., Mundy L.G., Wilking B.A., Hezel T., Blake G.F., 1994, ApJ 424, 222
- Raga A.C., Biro S., 1993, MNRAS 264, 758

- Raga A.C., Cantó J., Biro S., 1993, MNRAS 260, 163  
Raga A.C., Kofman L., 1992, ApJ 386, 222  
Raga A.C., Mellema G., Arthur S.J., et al., 1999, Rev. Mex. Astron. Astrofis. 35, 123  
Raga A.C., Navarro-González R., Villagrán-Muniz M., 2000, Rev. Mex. Astron. Astrofis. 36, 67  
Raga A.C., Noriega-Crespo A., 1998, AJ 116, 2943  
Reipurth B., Hartigan P., Heathcote S., Morse J.A., Bally J., 1997, AJ 114, 757  
Reipurth B., Heathcote S., Yu K.C., Bally J., Rodríguez L.F., 2000, ApJ 534, 317  
Rodríguez L.F., Curiel S., Moran J.M., et al., 1989, ApJ 346, L85  
Rodríguez L.F., Moran J.M., Ho P.T.P., Gottlieb E.W., 1980, ApJ 235, 845  
Snell R.L., Bally J., 1986, ApJ 303, 683  
Stone J.M., Norman M.L., 1994, ApJ 420, 237  
Torrelles J.M., Gómez J.F., Curiel S., et al., 1992, ApJ 384, L59  
Suttner G., Smith M.D., Yorke H.W., Zinnecker H., 1997, A&A 318, 595  
Völker R., Smith M.D., Suttner G., Yorke H.W., 1999, A&A 343, 953  
White G.J., Casali M.M., Eiroa C., 1995, A&A 298, 594  
Zeiner R., Eislöffel J., 1999, A&A 347, 565